

VORTA: Efficient Video Diffusion via Routing Sparse Attention

Wenhao Sun Rong-Cheng Tu[§] Yifu Ding Zhao Jin
Jingyi Liao Shunyu Liu Dacheng Tao[§]

Nanyang Technological University

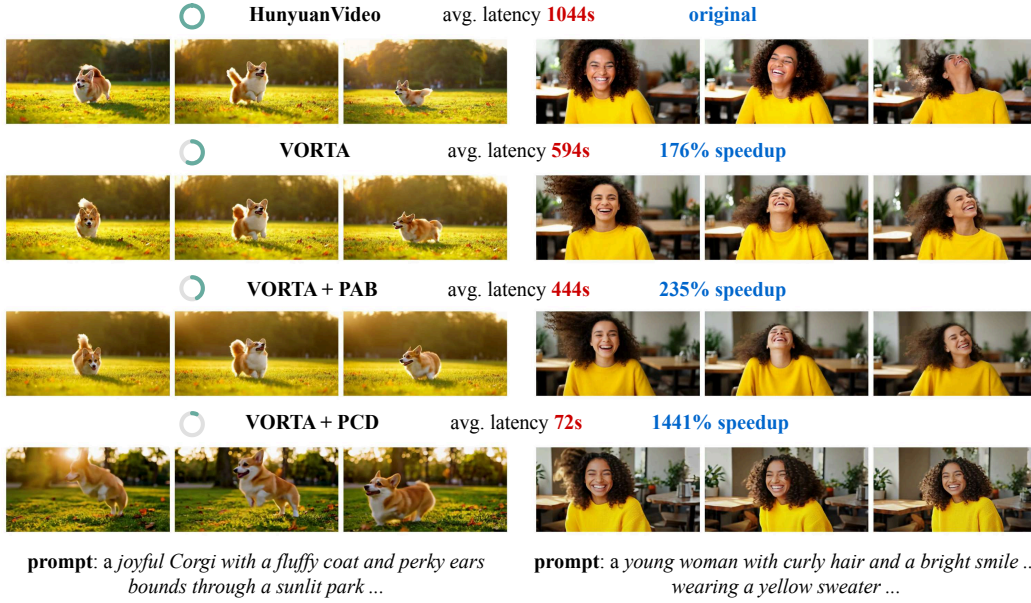


Figure 1: **VORTA** enables lossless acceleration of video diffusion transformers [13, 32], and remains compatible with other acceleration methods such as PAB [47] and PCD [33] for additional speedups.

Abstract

Video Diffusion Transformers (VDiTs) have achieved remarkable progress in high-quality video generation, but remain computationally expensive due to the quadratic complexity of attention over high-dimensional video sequences. Recent attention acceleration methods leverage the sparsity of attention patterns to improve efficiency; however, they often overlook inefficiencies of redundant long-range interactions. To address this problem, we propose **VORTA**, an acceleration framework with two novel components: (1) a sparse attention mechanism that efficiently captures long-range dependencies, and (2) a routing strategy that adaptively replaces full 3D attention with specialized sparse attention variants throughout the sampling process. It achieves a $1.76\times$ end-to-end speedup without quality loss on VBench. Furthermore, VORTA can seamlessly integrate with various other acceleration methods, such as caching and step distillation, reaching up to $14.41\times$ speedup with negligible performance degradation. VORTA demonstrates its efficiency and enhances the practicality of VDiTs in real-world settings.

[§] Co-corresponding authors: {rongcheng.tu, dacheng.tao}@ntu.edu.sg

1 Introduction

Video Diffusion Transformers (VDiTs) have demonstrated impressive video generation performance, producing realistic and dynamic content [13, 24, 32, 39]. Despite this progress, VDiTs remain computationally expensive due to the inherently high-dimensional nature of video data, compounded by the quadratic complexity of attention operations. For example, recent HunyuanVideo [13] requires almost 1000 seconds (500 PFLOPS) to generate a 5-second 720p video at 24 frames per second (FPS) on an H100 GPU. To mitigate the high sampling cost, studies [29, 33, 40] have proposed to enforce the self-consistency property of probability flow ODE (PF-ODE) [28] through distillation, achieving up to an $8\times$ reduction in sampling steps [44]. Other research [17, 20, 47] introduces caching intermediate features to accelerate sampling without additional training.

Another promising direction is to leverage the inherent locality in attention operations: attention scores tend to concentrate on a small subset of keys within a local window around each query, as shown in Figure 2 (left). The spatially nearest 4% of keys (4,000 out of 108,000) contribute over 80% of the total attention scores in HunyuanVideo [13]. In contrast, the remaining distant 96% of keys contribute less than 20% of the scores, yet dominate the computational cost of the attention operation. To address this inefficiency, many studies replace full attention with sliding window attention, which restricts interactions to nearby tokens and discards distant ones [1, 38, 41, 43]. Restricting computations to a small local subset of tokens enables a substantial speedup. But the locality assumption fails in many attention heads, as depicted in Figure 2 (left). Moreover, during the early sampling steps, the spatially nearest keys account for less than 40% of the total attention score in most attention heads, as shown in Figure 2 (right). These attention heads distribute interactions across the entire sequence, capturing global context and long-range dependencies that are critical for high-quality video generation [39].

However, efficient designs for long-range attention remain underexplored and represent a key bottleneck in accelerating VDiTs. Some studies [35, 43] adopt large attention windows or even full attention during stages with long-range dependencies, which offsets the overall acceleration. Other methods have tried to unify the modeling of short- and long-range dependencies using dynamic attention patterns [30, 34, 42], but their quadratic-time pattern detections/profiling introduce additional forward-pass complexity. Different from previous methods, we observed that most long-range interactions occur during the initial sampling steps. Figure 3 (middle) indicates that high-level semantic structures, such as spatial layouts and object motions, are primarily formed in this stage. This motivates our introduction of a sparse attention mechanism to substitute full attention when a compact coreset is sufficient to capture high-level semantics. We use a bucketed coreset selection (BCS) strategy to remove similar, redundant tokens and retain only the most representative ones for attention computation. As illustrated in Figure 3 (right), the output generated with coreset tokens during prediction retains semantic accuracy. Given that the coreset contains fewer tokens (e.g., 50% of the full sequence), the attention cost is reduced quadratically (e.g., to 25% of the original cost of the full sequence).

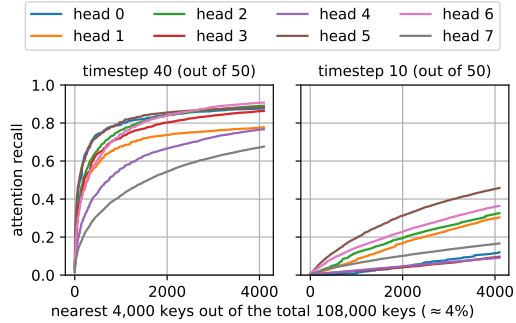


Figure 2: Attention scores recalled by the nearest keys. (left) Attention scores are predominantly concentrated within a local neighborhood. (right) The locality is less pronounced at earlier sampling steps. Results are from the 20th (of 60) layer in HunyuanVideo [13]. Only 8 out of the 24 attention heads are shown for clarity.

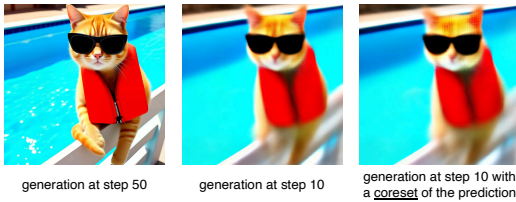


Figure 3: (left) Generation with the complete sampling process. (middle) Early sampling primarily captures high-level semantics before fine details appear. (right) Denoising based on a coreset of the predictions maintains semantic accuracy.

The attention patterns in VDiTs are affected by both the input signals and the knowledge embedded in weights. These patterns vary significantly across sampling steps and network parameters, making it challenging to integrate appropriate sparse attention variants into pretrained VDiTs. A naive approach is to log attention score distributions through a reverse diffusion sampling process and reuse them. However, this is impractical in real-world settings where sampling configurations (*e.g.*, video size or sampling steps) frequently change, rendering the logged patterns obsolete and requiring re-tuning. To overcome this, we introduce a VORTA routing mechanism that dynamically selects the optimal sparse attention variant by leveraging both the input signal-to-noise level and the pretrained knowledge encoded in each attention head. VORTA incurs only minimal overhead, adding a lightweight linear projection (0.1% of the total parameters) without requiring additional online profiling in prior methods [30, 34, 42]. It provides precise control and adaptable support for diverse diffusion configurations, offering greater flexibility than heuristic-based pattern detection methods [35, 43].

To conclude, our contributions are summarized as follows:

- We propose a novel coreset attention that effectively models long-range dependencies while theoretically reducing the attention cost by 75%.
- We introduce VORTA, an approach that integrates multiple sparse attentions into VDiTs for end-to-end acceleration without sacrificing performance. VORTA is compatible with various SDE/ODE solvers and network backbones.
- VORTA achieves up to a $1.76\times$ end-to-end speedup on VBench [9]. It is also compatible with other acceleration techniques, achieving overall speedups of up to $2.35\times$ with feature caching [47] and $14.41\times$ with consistency distillation [33].

2 Preliminary and related work

Flow matching and diffusion models. Flow Matching (FM) [16, 18] builds upon Continuous Normalizing Flows (CNFs) [3] and has since been integrated with the diffusion paradigm [8, 28], forming the foundation of many recent VDiTs [13, 24, 32]. The core concept of FM involves a time-dependent velocity field (VF) v_t and a time-dependent diffeomorphism $\mathbf{x}_t := t\mathbf{x}_1 + (1-t)\mathbf{x}_0$, known as a *flow*. The VF governs the evolution of the flow through an ordinary differential equation (ODE) $d\mathbf{x}_t = v_t(\mathbf{x}_t) dt$, where the flow \mathbf{x}_t defines a probability density path p_t , starting from the simple prior $p_0 = \mathcal{N}(\mathbf{0}, \mathbf{I})$ and evolving towards the intractable target density p_1 .

Lipman et al. [16] introduced Conditional Flow Matching (CFM) to optimize the neural network $v_t^\theta(\mathbf{x}_t)$ (*i.e.* VDiTs in this context) as follows:

$$\mathcal{L}_{\text{CFM}} = \mathbb{E}_{t, p_1(\mathbf{x}_1), p_0(\mathbf{x}_0)} \|v_t^\theta(\mathbf{x}_t) - (\mathbf{x}_1 - \mathbf{x}_0)\|^2. \quad (1)$$

Once optimized, it can start from $\mathbf{x}_0 \sim p_0$ and follow the ODE trajectory to generate samples.

3D self-attention of video diffusion transformers. Recent VDiTs [13, 24, 32, 39] employ 3D attention to capture spatio-temporal dependencies in video data. Given a video with F frames at a resolution of $H \times W$, the input is flattened into a sequence of length $L = F \times H \times W$, denoted as $\mathbf{H} \in \mathbb{R}^{L \times d}$, where each token is a d -dimensional vector. The self-attention is formulated as:

$$\text{attn}(\mathbf{H}) = \text{softmax}((\mathbf{H}\mathbf{W}_Q)(\mathbf{H}\mathbf{W}_K)^\top)(\mathbf{H}\mathbf{W}_V), \quad (2)$$

where $\mathbf{W}_Q, \mathbf{W}_K, \mathbf{W}_V \in \mathbb{R}^{d \times d}$ are the linear projection matrices. The attention operation is of complexity $\mathcal{O}(L^2d) + \mathcal{O}(Ld^2)$, where $d \ll L$ for high-resolution videos. Despite employing techniques such as Variational Autoencoders (VAEs) [12, 25] and patchification [23], the token count L still reaches up to 100K for a 5-second 720p video in HunyuanVideo [13]. Consequently, attention operations dominate the computational cost, accounting for over 75% of the computation cost. Optimizing the attention computation is crucial for the efficiency of VDiTs.

Video diffusion acceleration. General diffusion acceleration methods include step distillation [19, 21, 26, 27, 29, 33], which reduces the number of sampling steps to as few as 4 to 8 with sufficient tuning, and feature caching [11, 17, 20, 46, 47], which avoids redundant computation by reusing intermediate features. In the case of VDiTs, the long sequence length leads to high attention costs. As a result, many studies have focused on optimizing attention for long sequences. Some recent approaches [35, 43] apply predefined sparse attention patterns to reduce computational overhead.

Others [30, 34, 42] adopt online profiling to dynamically select attention patterns during inference. However, these sparse attention techniques depend on careful hyperparameter tuning for different configurations and/or introduce additional forward-pass complexity that offsets their speed benefits. VORTA addresses these challenges with a flexible design that is compatible with various diffusion configurations and model backbones, without incurring any additional inference-time overhead.

3 VORTA: efficient video diffusion via routing sparse attention

We introduce **VORTA**, our method to accelerate VDiTs. We begin with a taxonomy of attentions in Section 3.1. Next, we present two core components: i) sparse attention variants that speed up specific attentions (Section 3.2) ii) a routing strategy that integrates these sparse attentions into pretrained VDiTs for end-to-end acceleration (Section 3.3).

3.1 Taxonomy of VDiT attentions

The attention sparsity has been briefly discussed in Section 1. We formally categorize attentions in VDiTs into three types:

- **Quality attentions** focus on short-range interactions without attending to distant tokens. They are primarily responsible for fine-grained details during generation.
- **Semantic attentions** distribute their attention scores across the entire sequence. These attentions mainly capture high-level semantic information, including coarse layout and motion. Minor perturbations, such as merging similar tokens, are acceptable.
- **Pivotal attentions** maintain a global perceptual field while simultaneously refining local details. Small perturbations to these attentions can result in noticeable quality degradation.

All three types of attention coexist in VDiTs and are not mutually exclusive during the sampling: semantic attention may transition into quality attention as the diffusion process evolves, and vice versa. We will provide supporting evidence for this taxonomy through experimental results in Figure 8.

3.2 Sparse attentions

Sliding window for quality attentions. Sliding window attention [1, 41] proposes restricting each query token at position i to attend to its local neighborhood within the range $(i - w, i + w]$, where w is the window size. However, its zigzag-shaped attention mask introduces computation bubbles in block-wise kernel implementations (e.g., FlashAttention [4, 5]). This problem becomes more severe in three-dimensional video data, where the number of computation bubbles grows cubically. Zhang et al. [43] proposed sliding tile attention to tackle this problem. In the case of 1D attention, the attention mask is defined as: $\mathbf{M} = \{m_{i,j}\} = \{j \in [\text{tile_center}(i) - w, \text{tile_center}(i) + w]\}$, where $\text{tile_center}(i) = \lfloor i/t \rfloor \cdot t + \lceil t/2 \rceil$, and t is the tile size. It can be interpreted as shifting the window of non-center queries to align with the query in the center of the tile, as illustrated in Figure 4. The attention mask for sliding tile attention is block-wise dense and offers greater hardware efficiency. Our implementation employs 3D sliding tile attention to model local interactions of quality attentions with detailed pseudo code in Appendix A.1.

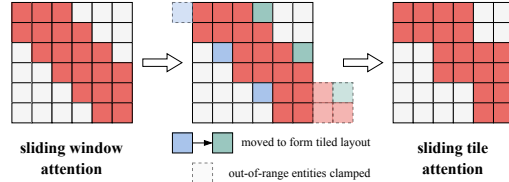


Figure 4: Illustration of converting a sliding window mask into a sliding tile mask. A 1D attention mask is shown for simplicity, with both the window size and tile size set to 2.

Coreset selection for semantic attentions. It is observed that many attentions with large perceptual fields are less sensitive to perturbations [30], corresponding to the semantic attentions defined earlier. We employ a coreset attention to capture such long-range interactions and accelerate computation by actively ignoring redundant features. A prototype coreset attention operation is defined as follows:

$$\text{coreset-attn}(\mathbf{H}) = \text{unpool} \circ \text{attn} \circ \text{pool}(\mathbf{H}), \quad (3)$$

where \circ denotes the composition operator, meaning the connected operators are applied sequentially from right to left. There are various valid approaches to define the $\text{pool}(\cdot)$ and $\text{unpool}(\cdot)$ operations,

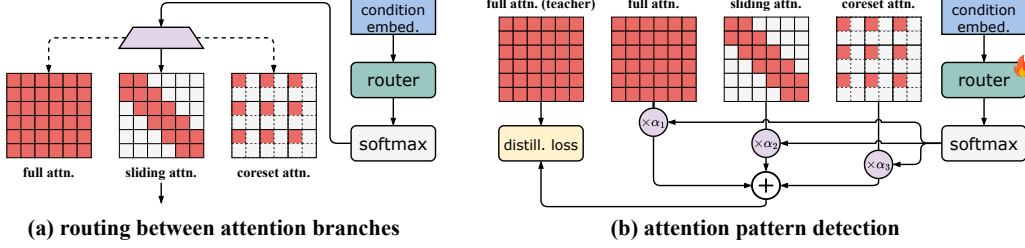


Figure 5: **Overview of VORTA.** 1D masks are used to represent the attention branches for simplicity. (a) During inference, the router takes the condition embedding as input and selects the appropriate attention branch. In this example, it activates sliding attention. (b) During pattern detection, all attention branches are activated, and their outputs are aggregated using gate values from the router. The divergence between the full attention output and the routed output is used to update the router.

provided they can compress a long sequence into a compact coreset and recover the original sequence length. However, standard average pooling assumes that all tokens within the pooling kernel are sufficiently similar to be merged. This assumption may not hold in practice, and such indiscriminate pooling can lead to a noticeable degradation in generation quality.

As an alternative, we implement the $\text{pool}(\cdot)$ operation using Bucketed Coreset Selection (BCS), as outlined in Algorithm 1. It offers greater flexibility and fidelity by selectively dropping redundant tokens. Specifically, the video tokens are divided into buckets of size (t, h, w) and the similarity is computed between each center token \mathbf{H}_i^c and its surrounding tokens \mathbf{H}_i^e within the i -th window. Given the size of the representative coreset for each bucket as $t \cdot h \cdot w \cdot r_{\text{core}}$, the $n_{\text{drop}} = t \cdot h \cdot w \cdot (1 - r_{\text{core}})$ non-center tokens with the highest similarity to the center are removed, and their information is represented by the center token. This design is motivated by the intuition that the center token is often very similar to its neighboring tokens. Even if this assumption does not hold, the remaining $(thwr_{\text{core}})$ tokens can complement the necessary information. In contrast to the global pairwise similarity computation for sequence reduction [2, 30], which has a $\mathcal{O}(L^2)$ complexity for sequence length L , our BCS achieves linear complexity $\mathcal{O}(L)$ by removing inter-bucket similarity computations. BCS demonstrates both high efficiency and strong performance in practice.

After applying the attention operation on the coreset tokens, we retrieve the original sequence by scattering the center token back to the dropped tokens for the subsequent operations. A detailed pseudo-code implementation and complexity analysis are provided in Appendix A.1.

3.3 Signal-aware attention routing and detection

Attention router. Our router adaptively selects the most suitable attention branch. For the n -th transformer block, we define a set of gate values, $\alpha^{(n)} = \{\alpha_i^{(n)}\}$, that quantify the importance of the full, sliding, and coreset attention branches, respectively. A lightweight router implemented as a linear layer that takes the diffusion timestep embedding $\mathbf{T} \in \mathbb{R}^d$ as input to capture the signal-to-noise level of the input features, followed by a softmax to produce the gate values:

$$\alpha^{(n)} = \text{softmax}(\mathbf{T}\mathbf{W}_R^{(n)}), \quad (4)$$

where $\mathbf{W}_R^{(n)} \in \mathbb{R}^{d \times 3}$ denotes the linear projection matrix. This lightweight design adds just 0.1% to the model’s parameters, while enabling the router to adaptively modulate gate values based on the current signal-to-noise ratio (SNR), without directly operating on the full set of diffusion tokens.

Algorithm 1 Bucketed Coreset Selection (BCS)

Input: bucket size (t, h, w) , coreset ratio r_{core} , input feature sequence \mathbf{H} .

- 1: $n_{\text{drop}} = t \cdot h \cdot w \cdot (1 - r_{\text{core}})$
- 2: $\mathbf{H}_1, \dots, \mathbf{H}_B \leftarrow \text{split_buckets}(\mathbf{H}, t, h, w)$
- 3: **for** $i \leftarrow 1$ to B **do**
- 4: $\mathbf{H}_i^c, \mathbf{H}_i^e \leftarrow \text{split_center}(\mathbf{H}_i)$
- 5: $\triangleright \text{len}(\mathbf{H}_i^c) = 1, \text{len}(\mathbf{H}_i^e) = thw - 1$
- 6: $\mathbf{S} \leftarrow \text{similarity}(\mathbf{H}_i^c, \mathbf{H}_i^e) \quad \triangleright \mathcal{O}(thw)$
- 7: $\text{idx} \leftarrow \text{topk_indices}(\mathbf{S}, k = n_{\text{drop}})$
- 8: $\tilde{\mathbf{H}}_i^e \leftarrow \text{drop_by_indices}(\mathbf{H}_i^e, \text{idx})$
- 9: $\triangleright \text{drop } n_{\text{drop}} \text{ most similar tokens}$
- 10: $\tilde{\mathbf{H}}_i \leftarrow \text{concat}(\mathbf{H}_i^c, \tilde{\mathbf{H}}_i^e)$
- 11: **end for**
- 12: $\tilde{\mathbf{H}} \leftarrow \text{concat}(\tilde{\mathbf{H}}_1, \dots, \tilde{\mathbf{H}}_B)$

Output: coreset feature sequence $\tilde{\mathbf{H}}$.

Inference-time routing strategy. The router activates the attention branch with the highest gate value, as illustrated in Figure 5 (a). It is formalized as a hard selection, defined as follows:

$$\mathbf{H}^{(n+1)} = \begin{cases} \text{sliding-attn}(\mathbf{H}^{(n)}) & \text{if } \alpha_2^{(n)} > \alpha_1^{(n)} \text{ and } \alpha_2^{(n)} > \alpha_3^{(n)} \\ \text{coreset-attn}(\mathbf{H}^{(n)}) & \text{if } \alpha_3^{(n)} > \alpha_1^{(n)} \text{ and } \alpha_3^{(n)} > \alpha_2^{(n)} \\ \text{attn}(\mathbf{H}^{(n)}) & \text{otherwise} \end{cases}, \quad (5)$$

where $\mathbf{H}^{(n)}$ represents the input features to the n -th transformer block. $\text{attn}(\cdot)$ is the standard full attention. $\text{sliding-attn}(\cdot)$ and $\text{coreset-attn}(\cdot)$ represent the sliding and coreset attentions, respectively, as defined in Section 3.2. Some operations, such as RoPE and FFN, have been omitted for clarity. Activating sparse attention branches yields a substantial speedup in attention computation. Although the full attention branch is activated in fewer than 0.2% of cases, it remains important for preserving model performance. We will empirically investigate these design choices in Section 4.3.

Attention pattern detection and router optimization. The remaining challenge is how to optimize the router to accurately identify attention patterns. Inspired by recent advances in language modeling [37], we adopt a self-supervised optimization strategy, as illustrated in Figure 5 (b). In the forward process, the gate values are employed to weight the outputs of the three branches:

$$\mathbf{H}^{(n+1)} = \alpha_1^{(n)} \cdot \text{attn}(\mathbf{H}^{(n)}) + \alpha_2^{(n)} \cdot \text{sliding-attn}(\mathbf{H}^{(n)}) + \alpha_3^{(n)} \cdot \text{coreset-attn}(\mathbf{H}^{(n)}). \quad (6)$$

We introduce a distillation loss $\mathcal{L}_{\text{distill}}$, defined as the MSE between the routed output $\mathbf{H}^{(N)}$ and the original output $\mathbf{H}_{\text{org}}^{(N)}$ of the final block, to ensure that the routed outputs remain close to the original model outputs to preserve the pretrained performance. In addition, we adopt the conditional flow matching loss \mathcal{L}_{CFM} from the VDiT pretraining stage as detailed in Section 2. To promote sparsity in routing decisions, we apply an L2 regularization term to gate values. The final loss function combines the conditional flow matching loss, the distillation loss, and the regularization term, weighted by hyperparameters λ_{distill} and λ_{reg} , respectively:

$$\mathcal{L} = \mathcal{L}_{\text{CFM}} + \lambda_{\text{distill}} \cdot \mathcal{L}_{\text{distill}} + \lambda_{\text{reg}} \cdot \mathcal{L}_{\text{reg}}, \quad (7)$$

$$\text{where } \mathcal{L}_{\text{distill}} = \text{MSE}(\mathbf{H}_{\text{org}}^{(N)}, \mathbf{H}^{(N)}) \text{ and } \mathcal{L}_{\text{reg}} = \sum_{n=1}^N \|\alpha_1^{(n)}\|^2. \quad (8)$$

Notably, the original parameters of the VDiTs are always frozen, and only the router is updated. We set $\lambda_{\text{distill}} = 20$ and $\lambda_{\text{reg}} = 0.02$ to balance the losses at a similar scale in our experiments. A detailed analysis of these hyperparameters is provided in Appendix B.1.

4 Experiments

4.1 Experiment setup

Baselines. This section presents the evaluation on the text-to-video generation task. We evaluate VORTA with two recently open-sourced VDiTs: HunyuanVideo [13] and Wan 2.1 [32]. Our comparisons include sparse attention acceleration methods: STA [43], which adopts a predefined sparse attention pattern, and ARnR [30], which performs online profiling to dynamically determine the sparse attention pattern. We also compare VORTA against two orthogonal approaches: the caching-based method PAB [47] and the step distillation method PCD [33]. Additionally, we report results for VORTA combined with PAB and PCD, as these methods can be integrated. For the Wan 2.1 [32], we only compare the pretrained baseline and VORTA, since other methods have not yet released code to support this model.

Benchmarks and evaluation metrics. Following prior works [30, 47], we evaluate on the standard VBench prompt suite [9], which contains over 900 text prompts across 16 dimensions. The primary performance metric is the aggregated VBench score. We also report the VBench quality and semantic subscores to provide a more detailed breakdown. To assess the deviation of generation from the pretrained models, we use LPIPS [45] as a reference metric. For efficiency analysis, we measure video sampling latency of the VDiTs, excluding the time required for text encoding and VAE decoding. We report the relative speedup as $\Delta\text{latency}/(\text{latency} + 1)$. Additionally, we record peak memory usage, which impacts practical deployment due to hardware constraints.

Table 1: Quantitative comparison under standard baseline settings (bf16, 720p, 5s). **C**: caching; **D**: step distillation; **S**: sparse attention.

Models	Type	VBench \uparrow	Quality \uparrow	Semantic \uparrow	LPIPS \downarrow	Latency (s)	Speedup	Mem. (GB)
HunyuanVideo [13]	-	82.26	83.68	76.60	-	1043.85	1.00×	47.64
+ ARnR [30]	S	82.39	83.85	76.56	0.211	790.55	1.32×	78.15
+ STA [43]	S	82.33	83.56	77.39	0.201	676.39	1.54×	51.79
+ PAB [47]	C	82.40	83.80	76.81	0.186	815.51	1.28×	> 80
+ VORTA	S	82.59	83.74	77.95	0.185	594.23	1.76×	51.15
+ VORTA & PAB	S & C	82.56	83.60	78.38	0.195	444.19	2.35×	> 80
+ PCD [33]	D	81.17	82.56	75.35	0.564	125.98	8.29×	47.64
+ VORTA & PCD	S & D	81.49	82.78	76.31	0.575	72.46	14.41×	51.15
Wan 2.1 (14B) [32]	-	82.36	83.05	79.60	-	1304.82	1.00×	41.77
+ VORTA	S	82.85	83.45	80.44	0.222	856.50	1.52×	43.97

Implementation. We implement VORTA in PyTorch [22], using FlexAttention kernel for sliding attention and FlashAttention [4, 5] kernel for all other attention operations. Video samples are generated in 50 steps, except for PCD [33], which uses 6 steps. The videos are 5 seconds long at 720p resolution. Due to out-of-memory issues with PAB [47] at this resolution, we adopt sequential CPU offloading [31]. For fair comparison, the latency introduced by model loading and offloading is excluded in the experiment results. For router optimization, we use the Mixkit dataset [15], training for 100 steps with a learning rate of 10^{-2} and a batch size of 4. All experiments are conducted on H100 GPUs with 80GB of memory. Additional implementation details are provided in Appendix A.2.

4.2 Main results

Performance. Table 1 presents the quantitative evaluation results of the baseline methods and VORTA. The key observations are: i) All methods maintain high VBench scores, except PCD, which shows a 1-point drop due to aggressive compression of generation steps. ii) VORTA, with and without PAB, ranks first and second in VBench score and LPIPS on HunyuanVideo, respectively. iii) The good performance of VORTA on both the MMdIT-based [7] HunyuanVideo and DiT-based [23] Wan 2.1 demonstrates its generalizability across diffusion backbones. Figures 1 and 6 quantitatively depict the generations produced by ARnR [30], STA [43], VORTA, VORTA & PAB [47], and VORTA & PCD [33] on HunyuanVideo. All variants maintain high visual quality with vivid appearance and coherent motion, consistent with the quantitative metrics. More qualitative comparisons and complete VBench dimensional scores are provided in Appendix B.4 and Appendix B.5, respectively.

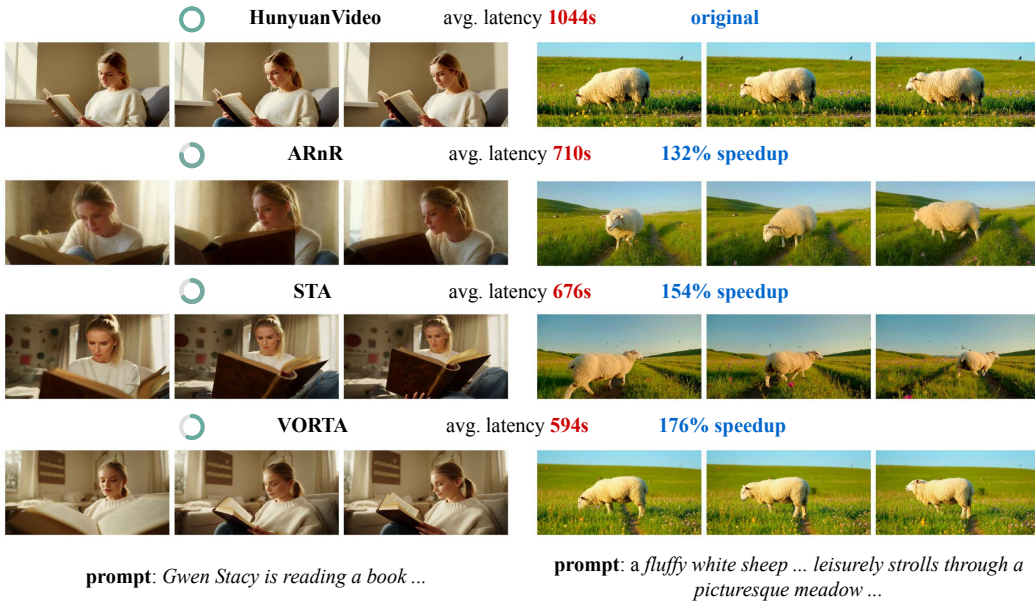


Figure 6: Qualitative comparison of sparse attention methods: ARnR [30], STA [43], and VORTA.

Efficiency. Among the sparse attention approaches, VORTA achieves the highest efficiency on HunyuanVideo, with a $1.76\times$ speedup. For the other line of work, PAB achieves a $1.28\times$ speedup on HunyuanVideo, but it requires over $1.7\times$ additional memory, which makes it less practical for large models or high-resolution videos. In practice, running PAB on an 80GB GPU necessitates sequential CPU offloading. The latency introduced by parameter loading and offloading nearly offsets the benefits of computation. The step distillation approach, PCD, achieves an $8.29\times$ speedup using only 6 sampling steps, with a mild drop in performance. While these methods offer different trade-offs in efficiency and performance, both can be effectively integrated with VORTA. When combined with PAB and PCD, VORTA achieves total speedups of $2.35\times$ and $14.41\times$, respectively.

Runtime breakdown. Figure 7 further presents the average latency of individual components for the sparse attention methods. Here, “attn.” denotes the isolated attention operation latency, whereas “attn. related” includes associated operations such as projections, RoPE, layer normalization, and other computations within the attention module.

Compared to ARnR [30], VORTA demonstrates superior efficiency. To preserve lossless generation, ARnR adopts a more conservative sparsity, resulting in higher latency in its “attn.” component. Furthermore, its $\mathcal{O}(L^2)$ similarity computation introduces additional latency, as evidenced by the larger latency in its “attn. related” component. In contrast, VORTA adaptively identifies efficient sparse patterns and allows greater speedups. Its coreset attention also involves similarity computation; however, BCS has only $\mathcal{O}(L)$ complexity, incurring negligible additional cost.

VORTA also outperforms STA [43], which uses a predefined sliding attention pattern. The main bottleneck of STA occurs during the first 15 sampling steps (see bottom two bars), when it must expand the window size to capture long-range dependencies. Consequently, these steps do not benefit from attention sparsity. In contrast, VORTA adaptively routes attention branches to accommodate diverse interaction types while maintaining near-constant latency across all diffusion steps.

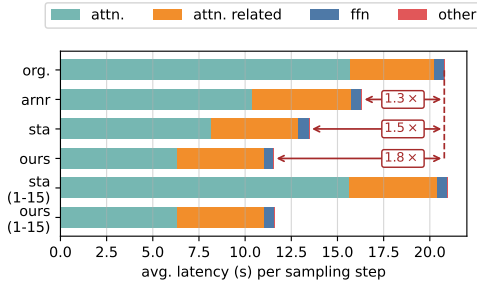


Figure 7: Runtime breakdown for sparse attention methods on HunyuanVideo [13].

Table 2: Evaluation of each VORTA component on Wan 2.1 (1.3B) [32].

Models	VBench \uparrow	Latency (s)	Speedup
Wan 2.1 (1.3B)	81.20	73.24	1.00 \times
w/o Sliding Attn.	80.25	65.14	1.12 \times
w/o Coreset Attn.	79.89	66.10	1.11 \times
w/o Full Attn.	77.14	59.34	1.23 \times
w/o Timestep Cond.	81.03	65.00	1.13 \times
w/ AP ₂₁₁	77.08	57.53	1.27\times
w/ AP ₁₂₁	76.01	57.64	1.27\times
w/ AP ₁₁₂	75.94	57.55	1.27\times
VORTA	81.06	58.42	1.25 \times

4.3 Ablation study

We conduct ablation studies on the Wan 2.1 (1.3B) [32] at its pretrained 480p resolution. All other experimental settings are identical to those used in the main experiment. At 480p, attention operation accounts for a smaller portion of the overall latency compared to 720p, resulting in less pronounced acceleration. Nevertheless, we adopt this smaller model and resolution to reduce the computational cost of benchmarking. The results are summarized in Table 2.

Attention branches. We evaluate the contribution of the attention branches individually by removing them. When the sliding attention branch is disabled, the router shifts more selections toward the full attention expert to preserve performance, resulting in an over 10% runtime increase, despite applying the same regularization level. Similarly, removing the coreset attention branch increases the latency by 14%. These results highlight the importance of both sparse branches in improving efficiency through the adaptive selection of attention patterns tailored to specific characteristics.

Given that the router selects the full attention branch in only 0.2% cases in VORTA (will be detailed in Section 4.4), we assess whether retaining it is necessary. As shown in Table 2, the removal of the full attention branch leads to a 4-point drop in the VBench score without any additional speedup. This suggests that the full attention branch remains crucial and validates the existence of the pivotal attention patterns defined in Section 3.1.

Timestep condition for signal-aware routing. We also examine the impact of including timestep information in attention routing. Removing the timestep embedding from the router input results in uniform attention branch selection across all diffusion steps, leading to slower 12%. In the absence of timestep conditioning, the router consistently selects the same attention expert. To maintain performance, the model predominantly routes to the full attention expert.

Bucketed coreset selection (BCS). We evaluate how much BCS improves performance compared to conventional average pooling. BCS sets the coreset size to 50% of the original sequence length. To ensure a fair comparison, we apply the same reduction ratio in the average pooling cases by configuring the pooling kernel sizes such that their product equals 2. To isolate the effect of compression along different dimensions, we evaluate three pooling kernel configurations: (2, 1, 1), (1, 2, 1), and (1, 1, 2), denoted as AP_{211} , AP_{121} , and AP_{112} , respectively. Although average pooling offers slightly lower latency by being free from similarity computations, its performance drops significantly. When adjacent tokens differ significantly, naive merging causes information loss, often resulting in artifacts such as pixelation or blurring in the generation.

4.4 Attention patterns in VDiTs.

Figure 8 illustrates the routed attention branch assigned to each head, layer, and sampling step. It reveals a clear temporal pattern: earlier time steps tend to use more coreset attention, while later time steps increasingly rely on sliding attention. Only a small fraction (about 0.2%) of attention heads are assigned to the full attention branch, highlighting the sparsity. As intuitively expected, earlier time steps likely focus on constructing high-level semantics rather than fine-grained details, whereas later time steps emphasize local interactions. Unlike auto-regressive or discriminative models [6, 10], VDiTs exhibit weaker layer-wise specialization; attention heads within the same layer are more evenly distributed across branches. A minor tendency is observed in later time steps where sliding attention is more frequently assigned to intermediate layers, while coreset attention is more often assigned to the initial and final layers. One plausible explanation is that intermediate layers capture local details, while subsequent layers refine the overall representation quality. Step-wise visualizations and results for other models are provided in Appendix B.3.

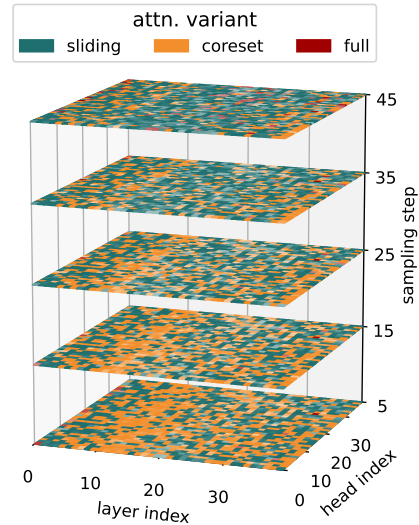


Figure 8: Optimized gate values for Wan 2.1 (14B) [32]. We visualize snapshots at sampling steps 5, 15, 25, 35, and 45 out of total 50 steps.

5 Conclusion

In this work, we presented VORTA, an efficient and generalized framework for accelerating diffusion transformers in video generation. VORTA reduces attention overhead by dynamically identifying attention patterns and routing them through appropriate sparse attention mechanisms. To further enhance efficiency, we introduced a bucketed coreset selection (BCS) strategy that improves the modeling of long-range dependencies. VORTA achieves a $1.76\times$ end-to-end speedup without compromising generation quality. Moreover, its high compatibility with existing acceleration techniques enables a combined speedup of up to $14.41\times$. We believe VORTA offers a practical and extensible solution, paving the way for broader adoption and future research in video generation.

Limitations. VORTA targets the attention mechanism, which accounts for over 75% of the total computation in high-resolution video generation. However, for tasks with short sequence lengths, such as image or low-resolution video generation, the attention overhead becomes less dominant. As a result, the potential acceleration achievable is limited. Additionally, this work focuses on the bidirectional generation paradigm. Other paradigms, such as autoregressive generation, are not directly supported and may require substantial adaptation. Additional discussion on failure cases, limitations, and border impacts is provided in Appendix C.

References

- [1] Iz Beltagy, Matthew E. Peters, and Arman Cohan. Longformer: The long-document transformer. *CoRR*, abs/2004.05150, 2020.
- [2] Daniel Bolya and Judy Hoffman. Token merging for fast stable diffusion. In *CVPR Workshops*. IEEE, 2023.
- [3] Tian Qi Chen, Yulia Rubanova, Jesse Bettencourt, and David Duvenaud. Neural ordinary differential equations. In *NeurIPS*, 2018.
- [4] Tri Dao. Flashattention-2: Faster attention with better parallelism and work partitioning. In *ICLR*, 2024.
- [5] Tri Dao, Daniel Y. Fu, Stefano Ermon, Atri Rudra, and Christopher Ré. Flashattention: Fast and memory-efficient exact attention with io-awareness. In *NeurIPS*, 2022.
- [6] Timothée Darcet, Maxime Oquab, Julien Mairal, and Piotr Bojanowski. Vision transformers need registers. In *ICLR*, 2024.
- [7] Patrick Esser, Sumith Kulal, Andreas Blattmann, Rahim Entezari, Jonas Müller, Harry Saini, Yam Levi, Dominik Lorenz, Axel Sauer, Frederic Boesel, Dustin Podell, Tim Dockhorn, Zion English, and Robin Rombach. Scaling rectified flow transformers for high-resolution image synthesis. In *ICML*. PMLR, 2024.
- [8] Jonathan Ho, Ajay Jain, and Pieter Abbeel. Denoising diffusion probabilistic models. In *NeurIPS*, 2020.
- [9] Ziqi Huang, Yanan He, Jiashuo Yu, Fan Zhang, Chenyang Si, Yuming Jiang, Yuanhan Zhang, Tianxing Wu, Qingyang Jin, Nattapol Chanpaisit, Yaohui Wang, Xinyuan Chen, Limin Wang, Dahua Lin, Yu Qiao, and Ziwei Liu. Vbench: Comprehensive benchmark suite for video generative models. In *CVPR*. IEEE, 2024.
- [10] Huiqiang Jiang, Yucheng Li, Chengruidong Zhang, Qianhui Wu, Xufang Luo, Surin Ahn, Zhenhua Han, Amir Abdi, Dongsheng Li, Chin-Yew Lin, Yuqing Yang, and Lili Qiu. Minference 1.0: Accelerating pre-filling for long-context llms via dynamic sparse attention. In *NeurIPS*, 2024.
- [11] Kumara Kahatapitiya, Haozhe Liu, Sen He, Ding Liu, Menglin Jia, Michael S Ryoo, and Tian Xie. Adaptive caching for faster video generation with diffusion transformers. *CoRR*, abs/2411.02397, 2024.
- [12] Diederik P. Kingma and Max Welling. Auto-encoding variational bayes. In *ICLR*, 2014.
- [13] Weijie Kong, Qi Tian, Zijian Zhang, Rox Min, Zuozhuo Dai, Jin Zhou, Jiangfeng Xiong, Xin Li, Bo Wu, Jianwei Zhang, Kathrina Wu, et al. Hunyuanvideo: A systematic framework for large video generative models. *CoRR*, abs/2412.03603, 2024.
- [14] Yaniv Leviathan, Matan Kalman, and Yossi Matias. Selective attention improves transformer. *CoRR*, abs/2410.02703, 2024.
- [15] Bin Lin, Yunyang Ge, Xinhua Cheng, Zongjian Li, Bin Zhu, Shadong Wang, Xianyi He, Yang Ye, Shenghai Yuan, Liuhan Chen, Tanghui Jia, Junwu Zhang, Zhenyu Tang, Yatian Pang, Bin She, Cen Yan, Zhiheng Hu, Xiaoyi Dong, Lin Chen, Zhang Pan, Xing Zhou, Shaoling Dong, Yonghong Tian, and Li Yuan. Open-sora plan: Open-source large video generation model. *CoRR*, abs/2412.00131, 2024.
- [16] Yaron Lipman, Ricky T. Q. Chen, Heli Ben-Hamu, Maximilian Nickel, and Matthew Le. Flow matching for generative modeling. In *ICLR*, 2023.
- [17] Feng Liu, Shiwei Zhang, Xiaofeng Wang, Yujie Wei, Haonan Qiu, Yuzhong Zhao, Yingya Zhang, Qixiang Ye, and Fang Wan. Timestep embedding tells: It’s time to cache for video diffusion model. *CoRR*, abs/2411.19108, 2024.
- [18] Xingchao Liu, Chengyue Gong, and Qiang Liu. Flow straight and fast: Learning to generate and transfer data with rectified flow. In *ICLR*, 2023.
- [19] Xingchao Liu, Xiwen Zhang, Jianzhu Ma, Jian Peng, and Qiang Liu. Instaflow: One step is enough for high-quality diffusion-based text-to-image generation. In *ICLR*, 2024.
- [20] Zhengyao Lv, Chenyang Si, Junhao Song, Zhenyu Yang, Yu Qiao, Ziwei Liu, and Kwan-Yee K. Wong. Fastercache: Training-free video diffusion model acceleration with high quality. *CoRR*, abs/2410.19355, 2024.
- [21] Chenlin Meng, Robin Rombach, Ruiqi Gao, Diederik P. Kingma, Stefano Ermon, Jonathan Ho, and Tim Salimans. On distillation of guided diffusion models. In *CVPR*. IEEE, 2023.

- [22] Adam Paszke, Sam Gross, Francisco Massa, Adam Lerer, James Bradbury, Gregory Chanan, Trevor Killeen, Zeming Lin, Natalia Gimelshein, Luca Antiga, Alban Desmaison, Andreas Köpf, Edward Z. Yang, Zachary DeVito, Martin Raison, Alykhan Tejani, Sasank Chilamkurthy, Benoit Steiner, Lu Fang, Junjie Bai, and Soumith Chintala. Pytorch: An imperative style, high-performance deep learning library. In *NeurIPS*, 2019.
- [23] William Peebles and Saining Xie. Scalable diffusion models with transformers. In *ICCV*. IEEE, 2023.
- [24] Adam Polyak, Amit Zohar, Andrew Brown, Andros Tjandra, Animesh Sinha, Ann Lee, Apoorv Vyas, Bowen Shi, Chih-Yao Ma, Ching-Yao Chuang, David Yan, et al. Movie gen: A cast of media foundation models. *CoRR*, abs/2410.13720, 2024.
- [25] Robin Rombach, Andreas Blattmann, Dominik Lorenz, Patrick Esser, and Björn Ommer. High-resolution image synthesis with latent diffusion models. In *CVPR*. IEEE, 2022.
- [26] Tim Salimans and Jonathan Ho. Progressive distillation for fast sampling of diffusion models. In *ICLR*, 2022.
- [27] Axel Sauer, Dominik Lorenz, Andreas Blattmann, and Robin Rombach. Adversarial diffusion distillation. In *ECCV*. Springer, 2024.
- [28] Yang Song, Jascha Sohl-Dickstein, Diederik P. Kingma, Abhishek Kumar, Stefano Ermon, and Ben Poole. Score-based generative modeling through stochastic differential equations. In *ICLR*, 2021.
- [29] Yang Song, Prafulla Dhariwal, Mark Chen, and Ilya Sutskever. Consistency models. In *ICML*. PMLR, 2023.
- [30] Wenhao Sun, Rong-Cheng Tu, Jingyi Liao, Zhao Jin, and Dacheng Tao. Asymrn: Video diffusion transformers acceleration with asymmetric reduction and restoration. *CoRR*, abs/2412.11706, 2024.
- [31] Patrick von Platen, Suraj Patil, Anton Lozhkov, Pedro Cuenca, Nathan Lambert, Kashif Rasul, Mishig Davaadorj, Dhruv Nair, Sayak Paul, William Berman, Yiyi Xu, Steven Liu, and Thomas Wolf. Diffusers: State-of-the-art diffusion models. <https://github.com/huggingface/diffusers>, 2022.
- [32] Ang Wang, Baole Ai, Bin Wen, Chaojie Mao, Chen-Wei Xie, Di Chen, Fei Wu Yu, Haiming Zhao, Jianxiao Yang, Jianyuan Zeng, Jiayu Wang, et al. Wan: Open and advanced large-scale video generative models. *CoRR*, abs/2503.20314, 2025.
- [33] Fu-Yun Wang, Zhaoyang Huang, Alexander William Bergman, Dazhong Shen, Peng Gao, Michael Lingelbach, Keqiang Sun, Weikang Bian, Guanglu Song, Yu Liu, Xiaogang Wang, and Hongsheng Li. Phased consistency models. In *NeurIPS*, 2024.
- [34] Haocheng Xi, Shuo Yang, Yilong Zhao, Chenfeng Xu, Muyang Li, Xiuyu Li, Yujun Lin, Han Cai, Jintao Zhang, Dacheng Li, Jianfei Chen, Ion Stoica, Kurt Keutzer, and Song Han. Sparse videogen: Accelerating video diffusion transformers with spatial-temporal sparsity. *CoRR*, abs/2502.01776, 2025.
- [35] Yifei Xia, Suhan Ling, Fangcheng Fu, Yujie Wang, Huixia Li, Xuefeng Xiao, and Bin Cui. Training-free and adaptive sparse attention for efficient long video generation. *CoRR*, abs/2502.21079, 2025.
- [36] Guangxuan Xiao, Ji Lin, Mickaël Seznec, Hao Wu, Julien Demouth, and Song Han. Smoothquant: Accurate and efficient post-training quantization for large language models. In *ICML*. PMLR, 2023.
- [37] Guangxuan Xiao, Jiaming Tang, Jingwei Zuo, Junxian Guo, Shang Yang, Haotian Tang, Yao Fu, and Song Han. Duoattention: Efficient long-context LLM inference with retrieval and streaming heads. *CoRR*, abs/2410.10819, 2024.
- [38] Guangxuan Xiao, Tianwei Yin, William T. Freeman, Frédo Durand, and Song Han. Fastcomposer: Tuning-free multi-subject image generation with localized attention. *IJCV*, 2025.
- [39] Zhuoyi Yang, Jiayan Teng, Wendi Zheng, Ming Ding, Shiyu Huang, Jiazheng Xu, Yuanming Yang, Wenyi Hong, Xiaohan Zhang, Guanyu Feng, Da Yin, Xiaotao Gu, Yuxuan Zhang, Weihang Wang, Yean Cheng, Ting Liu, Bin Xu, Yuxiao Dong, and Jie Tang. Cogvideox: Text-to-video diffusion models with an expert transformer. *CoRR*, abs/2408.06072, 2024.
- [40] Tianwei Yin, Michaël Gharbi, Richard Zhang, Eli Shechtman, Frédo Durand, William T. Freeman, and Taesung Park. One-step diffusion with distribution matching distillation. In *CVPR*. IEEE, 2024.
- [41] Manzil Zaheer, Guru Guruganesh, Kumar Avinava Dubey, Joshua Ainslie, Chris Alberti, Santiago Ontañón, Philip Pham, Anirudh Ravula, Qifan Wang, Li Yang, and Amr Ahmed. Big bird: Transformers for longer sequences. In *NeurIPS*, 2020.

- [42] Jintao Zhang, Chendong Xiang, Haofeng Huang, Jia Wei, Haocheng Xi, Jun Zhu, and Jianfei Chen. Spargeattn: Accurate sparse attention accelerating any model inference. *CoRR*, abs/2502.18137, 2025.
- [43] Peiyuan Zhang, Yongqi Chen, Runlong Su, Hangliang Ding, Ion Stoica, Zhenghong Liu, and Hao Zhang. Fast video generation with sliding tile attention. *CoRR*, abs/2502.04507, 2025.
- [44] Peiyuan Zhang, Runlong Su, Yongqi Chen, Hangliang Ding, William Lin, Kevin Lin, Wei Zhou, You Zhou, Yuzhou Nie, and Hao Zhang. Fastvideo is a lightweight framework for accelerating large video diffusion models. <https://github.com/hao-ai-lab/FastVideo>, 2025.
- [45] Richard Zhang, Phillip Isola, Alexei A. Efros, Eli Shechtman, and Oliver Wang. The unreasonable effectiveness of deep features as a perceptual metric. In *CVPR*. IEEE, 2018.
- [46] Wentian Zhang, Haozhe Liu, Jinheng Xie, Francesco Faccio, Mike Zheng Shou, and Jürgen Schmidhuber. Cross-attention makes inference cumbersome in text-to-image diffusion models. *CoRR*, abs/2404.02747, 2024.
- [47] Xuanlei Zhao, Xiaolong Jin, Kai Wang, and Yang You. Real-time video generation with pyramid attention broadcast. *CoRR*, abs/2408.12588, 2024.

VORTA: Efficient Video Diffusion via Routing Sparse Attention

Appendix

We organize the appendix as follows:

Methodological and implementation details:

- Appendix A.1: Methodological details
- Appendix A.2: Implementation details

Additional experimental results and findings:

- Appendix B.1: Hyperparameters analysis
- Appendix B.2: Runtime analysis
- Appendix B.3: Attention pattern analysis
- Appendix B.4: Qualitative comparison
- Appendix B.5: VBench dimensional scores

Limitations and border impact:

- Appendix C.1: Failure cases
- Appendix C.2: Border impact

A Methodology and implementation details

A.1 Methodological details

Sliding tile attention. Section 3.2 introduced the sliding tile attention [43], the sparse attention pattern we used to model local interactions. To keep the main text concise, we explained only the 1D case. Here, we present the 3D version of the sliding tile attention mask used in our implementation, as detailed in Algorithm 2.

Bucketed coreset selection (BCS). Section 3.2 also introduced the bucketed coreset selection (BCS) method, designed to reduce the computational overhead of modeling long-range interactions. In the naive setting, computing pairwise similarities across an input sequence of length L incurs a quadratic complexity of $\mathcal{O}(L^2)$. Bolya and Hoffman [2], Sun et al. [30] select a subset of tokens (e.g., 25%) as anchors and computing similarities between these anchors and the remaining tokens. This reduces the number of comparisons but still results in $\mathcal{O}((3L/4) \cdot (L/4)) = \mathcal{O}(L^2)$ complexity.

In contrast, BCS achieves linear complexity $\mathcal{O}(L)$ by employing a bucketing strategy. Each bucket, of size (t, h, w) , computes similarities between a central token and the remaining $(thw - 1)$ tokens, yielding a per-bucket cost of $\mathcal{O}(thw)$. With $L/(thw)$ such buckets, the total cost becomes $\mathcal{O}((L/(thw)) \cdot thw) = \mathcal{O}(L)$. No inter-bucket comparisons are performed, and the empirical results in Section 4.2 show that this approach is effective enough in selecting a representative subset of tokens for long-range interactions. Compared to global pairwise methods [2, 30], which require $\mathcal{O}(L^2)$ operations, BCS offers a substantially more efficient $\mathcal{O}(L)$ alternative.

A.2 Implementation details

Implementation details for our VORTA. Besides the implementation introduced in Section 4.1, we also provide the implementation details for our VORTA model.

For router optimization, we train on the Mixkit dataset [15] for 100 steps using a learning rate of 10^{-2} and a batch size of 4. Training completes in approximately one day using two H100 GPUs.

The sliding attention branch employs a window size of $(18, 27, 24)$, while the coreset attention branch uses a bucket size of $(2, 3, 2)$ with a coreset ratio of $r_{\text{core}} = 0.5$.

Algorithm 2 3D sliding tiled attention mask

Input: video size $\mathbf{v} = (F, H, W)$, tile size $\mathbf{t} = (t_F, t_H, t_W)$, window size $\mathbf{w} = (w_F, w_H, w_W)$.
1: *// Total sequence length for self-attention*
2: $L \leftarrow F \times H \times W$
3: $\mathbf{M} \leftarrow \mathbf{0}_{L \times L}$
4: *// The attention mask between the i -th query and the j -th key*
5: **for** $i \leftarrow 1$ to L **do**
6: **for** $j \leftarrow 1$ to L **do**
7: *// Get tile id from token id*
8: $q_F, q_H, q_W \leftarrow \text{get_tile_id_3d}(i, \mathbf{v}, \mathbf{t})$
9: $k_F, k_H, k_W \leftarrow \text{get_tile_id_3d}(j, \mathbf{v}, \mathbf{t})$
10: *// All queries within the same window share the same tile id as the window center tile id*
11: $q_F, q_H, q_W \leftarrow \text{get_window_center_id}(q_F, q_H, q_W, \mathbf{w})$
12: *// true if key tile is within the local window of query tile*
13: $m \leftarrow \text{bool}(\text{abs}(q_F - k_F) \leq w_F/2)$
14: $m \leftarrow m \text{ and } \text{bool}(\text{abs}(q_H - k_H) \leq w_H/2)$
15: $m \leftarrow m \text{ and } \text{bool}(\text{abs}(q_W - k_W) \leq w_W/2)$
16: *// Save the mask*
17: $\mathbf{M}[i, j] \leftarrow m$
18: **end for**
19: **end for**
Output: sliding tile attention mask \mathbf{M} .

Regarding video configurations during both training and inference, HunyuanVideo [13] utilizes videos with 117 frames at a resolution of 720×1280 (720p), while Wan 2.1 [32] uses 77-frame videos at the same resolution. For rendering, HunyuanVideo outputs videos at 24 frames per second (FPS), whereas Wan 2.1 generates videos at 15 FPS, as specified in their respective repositories.

Implementation details for baseline methods. To evaluate efficiency, the PAB [47] is tested on 720p videos from HunyuanVideo [13], aligning with the setup used in other methods. However, processing at this resolution with PAB requires over 80 GB of GPU memory. To address this limitation, we apply sequential CPU offloading [31]. For a fair comparison, we exclude the latency caused by model loading and offloading from the reported results. Despite this, the end-to-end runtime with CPU offloading exceeds 2000 seconds per video, which is substantially slower than the original pretrained model and offers no practical efficiency advantage. The original STA kernel supports video generation only at a fixed resolution of 768×1280 , which exceeds the 720p resolution used by the pretrained model. To ensure consistency in evaluation, we reimplemented the kernel using FlexAttention to support 720p video generation.

Evaluation metrics. To evaluate how the generated outputs differ from those of pretrained models, we use LPIPS [45] as a reference metric. However, since the pretrained models do not represent the ground truth, divergence from them does not necessarily indicate degraded performance. Multiple generated outputs may be equally valid, provided they align with the input prompts. LPIPS is only used as a comparative reference. The primary evaluation of video quality and prompt alignment should be based on VBench [9] scores.

The improved performance of acceleration methods. Interestingly, despite using less computation, VORTA slightly outperforms the original pretrained models in terms of VBench score. Similar findings have been reported in other acceleration methods [14, 36]. A possible explanation lies in the redundancies present in overparameterized models, which can introduce marginal negative effects. By pruning these redundancies, these acceleration methods may contribute to slight performance gains, although they are not intended for this purpose.

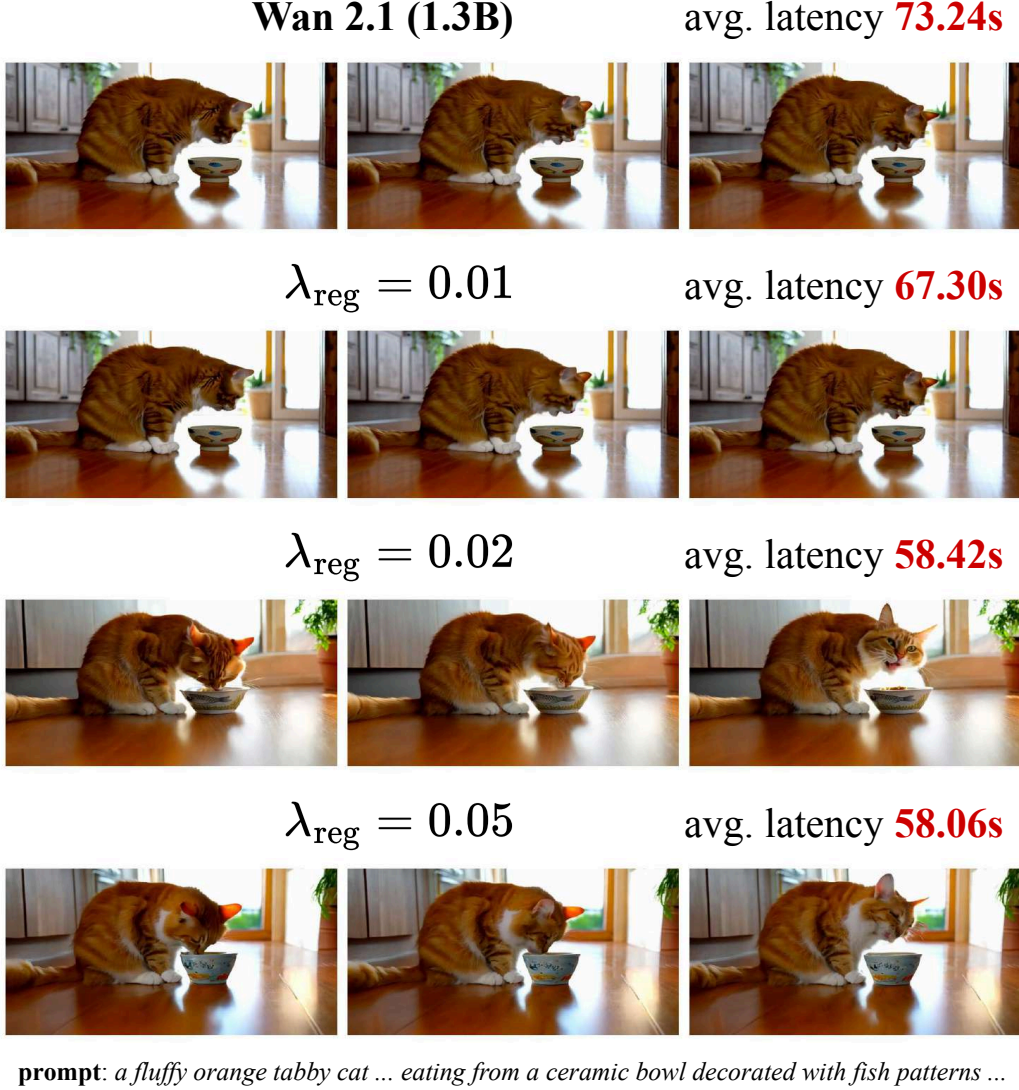


Figure 9: Qualitative evaluation of varying the regularization weight λ_{reg} .

B Additional experimental results and findings

B.1 Hyperparameters analysis

Figure 9 shows the effect of varying the regularization weight λ_{reg} . When λ_{reg} is small ($\lambda_{\text{reg}} = 0.01$), the speedup is limited, and in most scenarios, the router tends to select full attention. In contrast, with a large $\lambda_{\text{reg}} = 0.05$, the video exhibits noticeable distortion (e.g., the cat’s head in the final frame). A moderate value of $\lambda_{\text{reg}} = 0.02$ achieves a good trade-off between acceleration and output quality.

Figure 10 provides further analysis of alternative pooling strategies in the coreset attention branch. Using average pooling with a $r_{\text{core}} = 50\%$ coreset ratio significantly underperforms compared to BCS pooling, primarily because it lacks a selection mechanism. As the coreset ratio r_{core} increases, the VBench score improves; however, a ratio of $r_{\text{core}} = 50\%$ is sufficient to achieve strong performance. Higher ratios yield marginal performance gains while introducing additional computational overhead during generation.

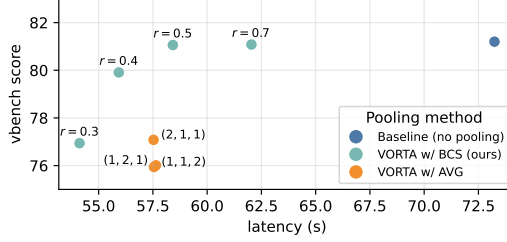


Figure 10: Effect of varying the coreset size in BCS and the kernel size in average pooling.

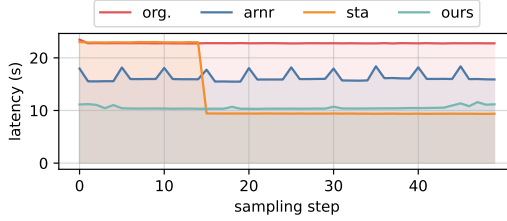


Figure 11: Per-step sampling latency on HunyuanVideo [13]. ARnR [30] yields smaller speedups overall. STA [43] shows no speedup in early timesteps.

B.2 Runtime analysis

Section 4.2 analyzed the average runtime (over diffusion steps) of each component, as shown in Figure 7. Figure 11 further presents the runtime breakdown per diffusion step. Overall, ARnR exhibits relatively high runtime, primarily due to limited acceleration in attention operations. Additionally, its periodic global similarity computation, with $\mathcal{O}(L^2)$ complexity, introduces a bottleneck. This is evident from latency spikes every five steps. In contrast, STA shows significantly higher runtime during the initial 15 steps due to the lack of early-stage acceleration, leading to reduced overall efficiency. Our VORTA achieves near-constant runtime across all steps, demonstrating stable and efficient performance.

B.3 Attention pattern analysis

Figures 12 and 13 show the router gate values for Hunyuan [13] and Wan 2.1 (14B) [32], respectively, as supplementary results for Section 3.1.

B.4 Qualitative comparison

In addition to the qualitative results in Figures 1 and 6 and the quantitative results in Table 1, we present further visualizations for Wan 2.1 (14B) in Figure 14. VORTA inherits the strong performance of the pretrained ViTs while offering a significant speedup.

B.5 VBench dimensional scores

VBench evaluates the generated videos across 16 dimensions. Due to space constraints, we report only three aggregated scores in Table 1, with the complete set of scores provided in Table 3 for completeness.

C Limitations and border impact

C.1 Failure cases

VORTA does not modify the pretrained parameters of VDiTs, and therefore its performance inherently depends on the quality of the underlying pretrained model. As illustrated in Figure 15,

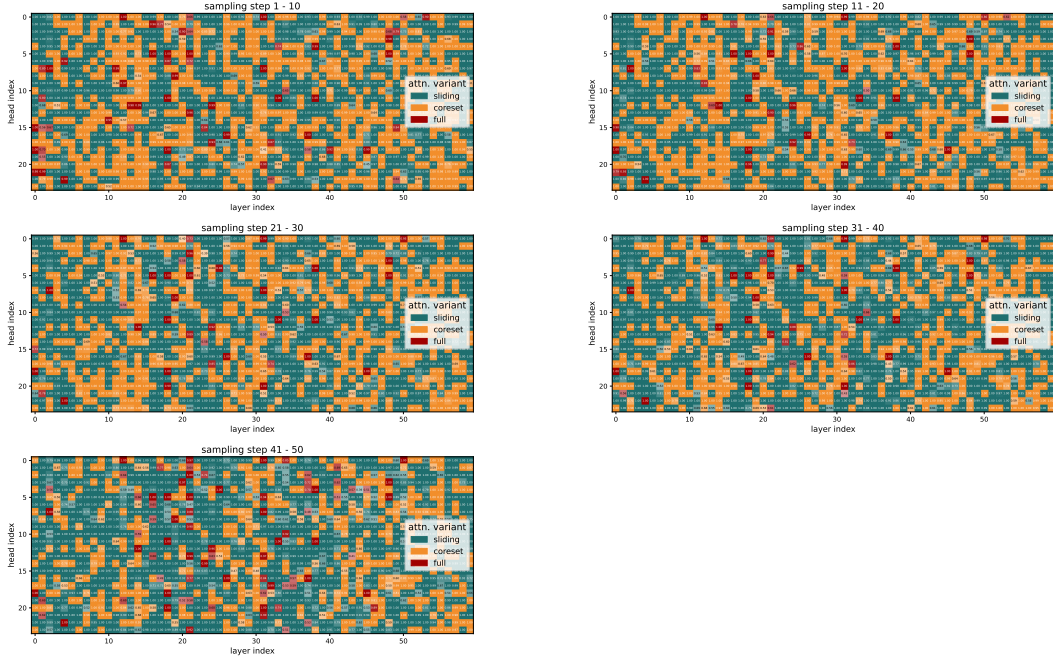


Figure 12: Optimized gate values for HunyuanVideo [13]. The 50 sampling steps are grouped into 5 equal intervals, and the averaged gate value within each interval is reported. Each color corresponds to a distinct attention branch, with color intensity indicating confidence.

Table 3: Quantitative results for VBench dimensions [9] for HunyuanVideo [13] and Wan (14B) [32].

Method	Aesthetic Quality \uparrow	Appearance Style \uparrow	Background Consistency \uparrow	Color \uparrow	Dynamic Degree \uparrow	Human Action \uparrow	Imaging Quality \uparrow	Motion Smoothness \uparrow
HunyuanVideo	62.05	77.88	93.80	91.35	38.89	96.00	63.33	96.98
+ ARnR	62.58	80.36	93.99	87.54	39.77	93.73	63.21	96.12
+ STA	63.87	79.48	94.47	86.39	39.58	97.00	61.92	96.79
+ PAB	63.53	75.85	94.82	87.92	36.11	98.00	63.40	97.34
+ VORTA	62.33	80.63	94.62	92.13	37.50	97.00	63.16	95.84
+ VORTA & PAB	63.16	80.43	95.22	90.92	36.31	97.50	62.05	96.18
+ PCD	62.69	76.21	94.44	85.94	31.94	94.00	63.08	96.46
+ VORTA & PCD	61.43	76.92	94.87	89.33	35.42	98.00	62.42	95.11
Wan 2.1 (14B)	63.33	82.12	94.55	83.26	37.50	99.00	63.99	91.60
+ VORTA	63.79	83.32	95.28	87.04	39.58	100.00	63.07	92.17

Method	Mutiple Objects \uparrow	Objects Class \uparrow	Overall Consistency \uparrow	Scene \uparrow	Spatial Relationship \uparrow	Subject Consistency \uparrow	Temporal Flickering \uparrow	Temporal Style \uparrow
HunyuanVideo	52.21	84.41	74.30	65.59	78.06	90.30	98.57	69.61
+ ARnR	52.09	87.49	69.88	69.21	80.89	90.55	99.28	70.70
+ STA	56.55	87.82	75.01	64.08	80.60	88.12	98.40	69.59
+ PAB	56.86	84.97	74.97	63.91	78.34	90.89	98.61	70.50
+ VORTA	58.00	89.56	74.62	61.87	78.30	92.43	98.47	69.44
+ VORTA & PAB	59.17	89.90	75.82	62.99	77.43	92.27	97.96	70.29
+ PCD	54.04	81.88	75.07	66.03	74.48	90.64	97.37	70.52
+ VORTA & PCD	51.07	85.05	74.93	67.09	73.70	91.34	97.50	70.69
Wan 2.1 (14B)	74.62	86.47	75.49	64.70	79.16	91.21	97.69	71.54
+ VORTA	75.76	88.45	75.09	63.29	80.28	90.76	97.78	70.70

when the pretrained VDiTs fail to generate high-quality videos, resulting in distortions or non-physical outputs, VORTA exhibits similar deficiencies. In some cases, it even produces outputs of lower quality than the original VDiTs. This degradation is attributed to computations on erroneous generations, which amplify distortions in the resulting videos.

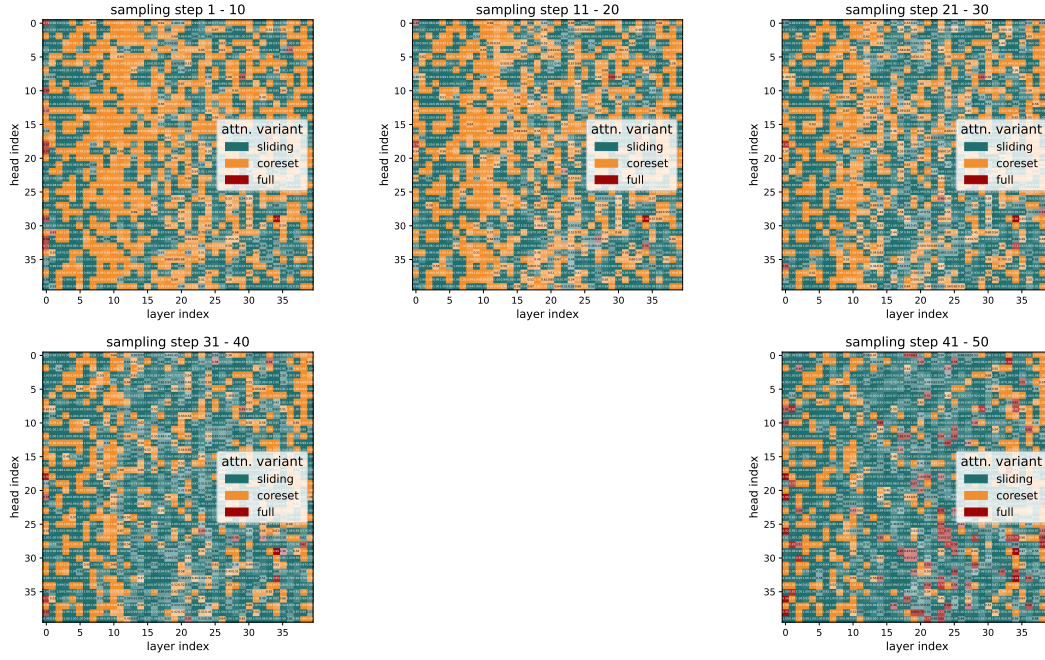


Figure 13: Optimized gate values for Wan 2.1 (14B) [32].

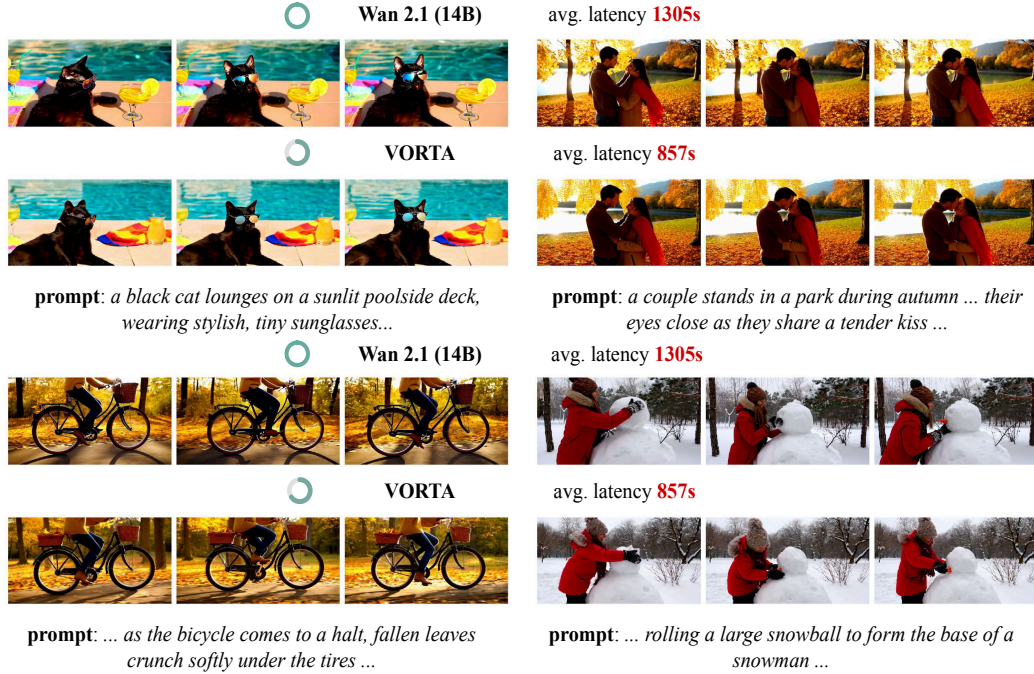


Figure 14: Qualitative comparison on Wan 2.1 (14B) [32].

C.2 Border impact

Generative models pose risks of producing biased, privacy-invasive, or harmful content. While our method accelerates video generation, it may also propagate such risks. It is imperative that researchers, developers, and platform providers actively assess and mitigate these potential harms to promote responsible use.

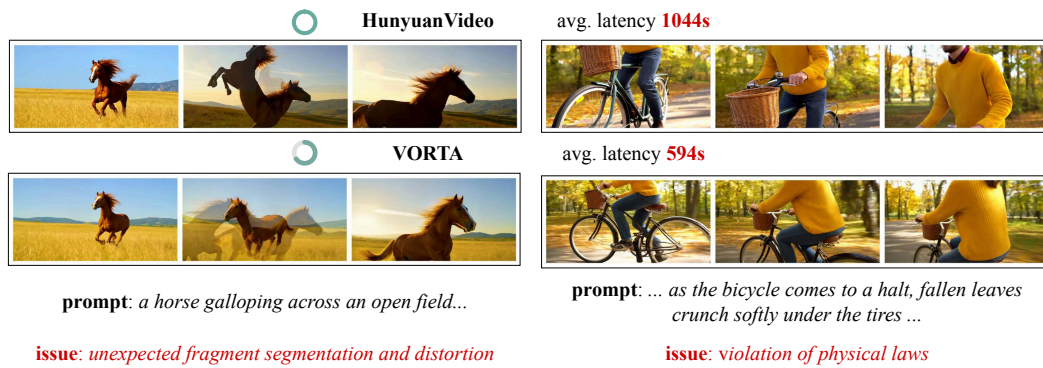


Figure 15: Failure cases. When the pretrained model exhibits distortions or non-physical phenomena, VORTA inherits these issues. We refer the reader to the supplementary video for a more illustrative example.